*Acta Cryst.* (1953). **6**, 846

# Structure Analysis of Single Crystals by Electron Diffraction. III. Modifications of Alumina

BY J. M. COWLEY

*Chemical Physics Section, Division of Industrial Chemistry, Commonwealth Scientific and Industrial Research Organization, Melbourne, Australia*

(*Received* 31 *March* 1953 *and in revised form* 4 *June* 1953)

An electron-diffraction study of the oxide films formed by heating aluminium foil in air on metal grid supports has revealed the occurrence of a number of new phases arbitrarily designated the $\lambda$, $\mu$, $\nu$, $\xi$ and $\xi'$ phases. Except for the $\lambda$-phase, all these phases may be indexed in terms of hexagonal unit cells with $a \sim 5$ Å and $c \sim 14$ Å, and appear to be intermediate between the $\alpha$- and $\gamma$-alumina phases. The $\lambda$-phase is orthorhombic, pseudo-tetragonal, with $a = b = 7{\cdot}63$ and $c = 2{\cdot}89$ Å and has a superlattice with a unit cell containing 14 normal unit cells. Poor-quality single-crystal patterns of the $\lambda$-phase have been used in the structure analysis of the average unit cell and the superlattice unit cell as a demonstration of the amount of information which can be derived from imperfect single-crystal patterns and of the effectiveness of image-seeking methods in the interpretation of Patterson projections obtained from electron-diffraction data. The [001] projection of the average unit cell was refined by using the values of $\frac{1}{2}(E'_{hk}+E^2_{hk}/E'_{hk})$ as Fourier coefficients, the $E'_{hk}$ being the structure factors calculated for the approximate structure found by image-seeking. The composition of the $\lambda$-phase is approximately $3NiO.5Al_2O_3$.

## 1. Introduction

The techniques involved in the application of Fourier methods to the structure analysis of very small single crystals using single-crystal electron-diffraction patterns, have been described in Part I of this series (Cowley, 1953*b*). An example of the results which can be obtained when good single-crystal patterns are available and when intensities are measured with moderate accuracy is the investigation of the configuration of the hydrogen bonds in boric acid, described in Part II (Cowley, 1953*c*). However, these methods may also be profitably applied when the only single-crystal patterns available are poor in quality and confused by the occurrence of many arcs, spots and portions of single-crystal patterns from neighbouring material, so that only very approximate values of the relative intensities, based on visual estimates, can be obtained. To illustrate the amount of information about an unknown structure which can be derived in such a case, the present paper describes the analysis, by a combination of image-seeking and Fourier methods, of the atomic distribution in the average unit cell and the superlattice unit cell of one of the modifications of alumina, referred to as the $\lambda$-phase, formed by heating a thin aluminium foil in air on a metal grid support.

Pieces of aluminium foil were thinned, until they were on the point of disintegrating, by floating them on a caustic soda solution. They were then picked up on a fine metal gauze or a wire loop, washed, and heated in air at temperatures ranging from 400 to 700° C. for periods of up to 50 hr. They were examined in the electron-diffraction camera by transmission methods, using a fine electron probe focused on the specimen so that patterns were obtained from areas of only a few microns diameter.

The camera was calibrated at intervals during the course of the experiments, using the sharp (00*l*) rings of ZnO and (*h*00) rings of MgO as reference standards. It is estimated that the errors in the absolute magnitudes of the unit-cell dimensions derived do not exceed $\frac{1}{2}$%, and the errors in the relative magnitudes obtained from any one plate are much smaller.

The most commonly occurring patterns consisted of rings and single-crystal reflexions from the well-known $\gamma$-alumina phase. The indication of stacking faults in this phase has been described previously (Cowley, 1953*a*). Patterns characteristic of other phases, not previously reported, were observed to become more prominent with increased heating time. These phases have been designated by arbitrary Greek letters. Their occurrence depended to some extent on the conditions of heating, and in some cases, on the nature of the metal supporting grid. The characteristics of the best-defined of these phases will be summarized briefly.

## 2. New alumina phases

### (1) *λ-phase*

This phase occurs when aluminium foil is heated in air at 450–600° C. on a nickel supporting grid, but not when a stainless steel or platinum grid or an open wire loop is used. The characteristic patterns were observed when aluminium foil on a platinum grid was sprinkled with fine nickel filings and then heated. An examination of such a specimen with an optical microscope

Table 1. *Ring patterns for new alumina phases*

λ-phase

| $d_o$ (Å) | $I$ | $hkl$ |
|---|---|---|
| 5·47 | *ms* | 110 |
| 3·45 | *s* | 210 |
| 2·87 | *w* | 001 |
| 2·69 | *ms* | 101, 220 |
| 2·55 | *ms* | 111, 300 |
| 2·42 | *mw* | 310 |
| 2·30 | *m* | 201 |
| 2·20 | *ms* | 211 |
| 2·11 | *mw* | 320 |
| 1·98 | *vw* | 221 |
| 1·895 | *mw* | 400, 301 |
| 1·845 | *m* | 410, 311 |
| 1·792 | *w* | 330 |
| 1·711 | *m* | 420, 321 |
| 1·596 | *w* | 401 |
| 1·568 | *vw* | 411 |
| 1·521 | *mw* | 430, 331 |
| 1·471 | *m* | 421 |
| 1·448 | *w* | 002 |
| 1·398 | *vw* | 112 |
| 1·353 | *vw* | 440, 202 |
| 1·331 | *mw* | 212, 511 |
| 1·317 | *vw* | 530 |
| 1·270 | *ms* | 600, 222 |

μ-phase

| $d_o$ (Å) | $I$ | $hkl$ |
|---|---|---|
| 4·84 | *m* | 100 |
| 4·58 | *mw* | 003 |
| 3·91 | *vw* | 102 |
| 3·56 | *vw* | 004 |
| 2·818 | *s* | 110 |
| 2·74 | *vw* | 111 |
| 2·55 | *w* | 112 |
| 2·42 | *m* | 105, 200 |
| 2·30 | *w* | 202 |
| 2·07 | *vw* | 106 |
| 1·99 | *mw* | 204 |
| 1·625 | *w* | 300 |
| 1·473 | *vw* | 118 |
| 1·406 | *ms* | 220 |
| 1·337 | *vw* | 310 |

ξ-phase

| $d_o$ (Å) | $I$ | $hkl$ |
|---|---|---|
| 4·24 | *vw* | 100 |
| 4·01 | *vw* | 101 |
| 3·62 | *m* | 102 |
| 2·66 | *m* | 104 |
| 2·475 | *s* | 110 |
| 2·17 | *m* | 113 |
| 2·05 | *w* | 202 |
| 1·82 | *m* | 204 |
| 1·671 | *mw* | 116 |
| 1·610 | *vw* | 211 |
| 1·580 | *w* | 212 |
| 1·467 | *mw* | 214 |
| 1·432 | *m* | 300 |
| 1·302 | *vw* | 10,10 |
| 1·240 | *w* | 220 |
| 1·192 | *w* | 223 |
| 1·169 | *vw* | 218 |
| 1·123 | *w* | 314 |
| 1·090 | *w* | 315 |

ν-phase

| $d_o$ (Å) | $I$ | $hkl$ |
|---|---|---|
| 4·85 | *w* | 100 |
| 4·09 | *m* | 101 |
| 2·83 | *vs* | 102, 110 |
| 2·44 | *mw* | 200, 003 |
| 2·035 | *m* | 202 |
| 1·84 | *w* | 004, 210 |
| 1·63 | *m* | 212 |
| 1·41 | *mw* | 220 |
| 1·32 | *w* | 303 |
| 1·27 | *w* | 214, 115 |
| 1·16 | *w* | 215 |

revealed small regions of discoloration of the aluminium oxide film about the points of contact with the nickel. Thus it seems probable that the λ-phase results from a reaction between the aluminium and nickel oxides. Evidence from the structure analysis, to be described later, also suggests that the phase contains nickel. No reference can be found in the literature to any reaction between alumina and nickel oxide at a temperature of less than 700° C., at which temperature the spinel $NiAl_2O_4$ is said to be formed (Krause & Thiel, 1932).

Continuous-ring patterns and many extensive single-crystal spot patterns were observed. The unit cell is orthorhombic, but pseudo-tetragonal with $a = b = 7{\cdot}63$, $c = 2{\cdot}89$ Å. Diffuse spots in the single-crystal patterns indicate that there is a superlattice with a unit cell containing 14 normal unit cells. Details of the ring pattern are given in Table 1. The $hk0$ single-crystal spot pattern is shown in Fig. 1, and the $2h,k,h$ pattern in Fig. 2.

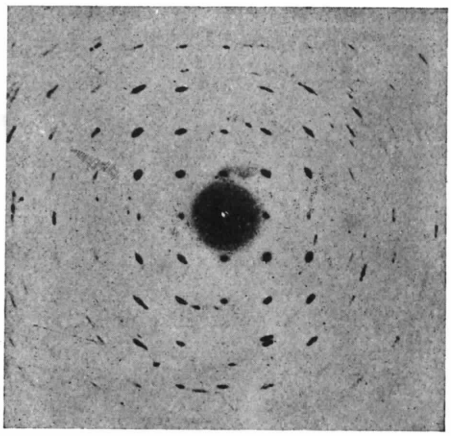

Fig. 1. Imperfect single-crystal pattern of $hk0$ spots of the λ-phase.

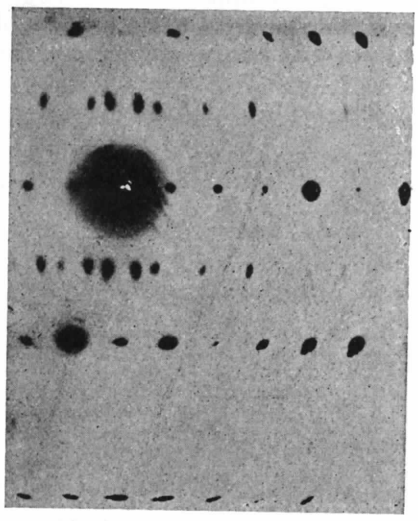

Fig. 2. Portion of a single-crystal pattern of $2h,k,h$ spots of the λ-phase, showing rows of diffuse superlattice spots

Fig. 3. Portion of a spotty-ring pattern of the $\xi$-phase, showing the fine structure of single-crystal spots.

(2) *$\mu$-phase*

This phase gives rather spotty rings when aluminium foil is heated to about 450° C. on nickel gauze. Details of the ring pattern are given in Table 1. The rings may be indexed in terms of a hexagonal unit cell with $a = 5{\cdot}60$, $c = 13{\cdot}67$ Å.

(3) *$\xi$-phase*

Sharp, bright patterns of spots, frequently containing extensive single-crystal patterns, characterize this phase. It is produced when aluminium foil is heated in air for long periods at 600–700° C. It has been observed with supporting gauzes of nickel, stainless steel and platinum. Patterns focused on the photographic plate (Fig. 3) consist of spotty rings with the individual spots drawn out into streaks and showing fine-structure rather similar to that observed for zinc oxide smoke (see e.g. Cowley & Rees, 1947). The rings are tabulated in Table 1. The unit cell is hexagonal with $a = 4{\cdot}98$, $c = 13{\cdot}52$ Å. The spot patterns indicate that multiples of this unit cell sometimes occur. On occasions the appearance of a large multiple unit cell is simulated by the occurrence of strong secondary diffraction effects, suggesting that two or more thin sheets of the material are superimposed with some definite orientational relationship. The details of the fine-structure of the individual spots of the spotty-ring patterns suggest that this phase crystallizes more commonly in the form of long thin spines, with the $c$ axis of the unit cell parallel to the long axis of each spine.

(4) *$\xi'$-phase*

This phase sometimes occurs with the $\xi$-phase. Apart from a few $hk0$ spot patterns (Fig. 4) which give $a = 5{\cdot}23$ Å, and usually show evidence of distortion of the lattice, a few spot patterns were observed from which the $c$-axis could be estimated to be approximately $c = 7{\cdot}06$ Å, but no ring patterns could be obtained.

(5) *$\nu$-phase*

Ring patterns and extensive spot patterns (Fig. 5) of this phase were obtained by heating aluminium foil, mounted on a nickel gauze or wire loop, for a few seconds at bright red heat in a Bunsen oxidizing flame. The rings (Table 1) and spot patterns indicated a hexagonal cell with $a = 5{\cdot}53$, $c = 7{\cdot}16$ Å.

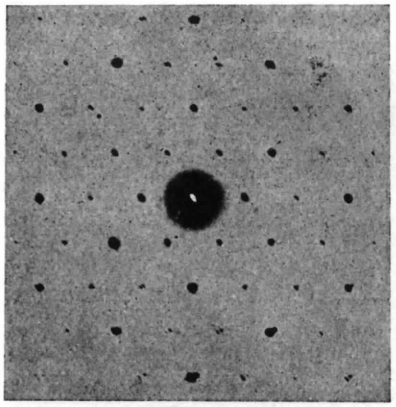

Fig. 4. Single-crystal pattern of $hk0$ spots of the $\xi'$-phase.

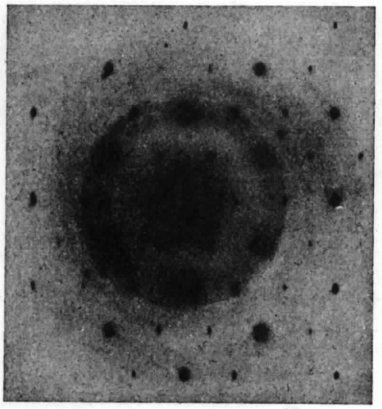

Fig. 5. Single-crystal $hk0$ spot pattern and diffuse rings of the $\nu$-phase.

It is to be noted that, if the $c$ axes of the $\xi'$ and $\nu$ phases are doubled, all the above phases, except the $\lambda$-phase, may be described in terms of a hexagonal cell with $a \sim 5$ Å and $c \sim 14$ Å. The $\alpha$-phase (rhombohedral) and the $\gamma$-phase (cubic) may also be described in terms of hexagonal cells with dimensions of the same order. In Table 2 the dimensions, axial ratios

Table 2. *Comparison of equivalent hexagonal unit cells for various phases of alumina*

| Phase | $a$ (Å) | $c$ (Å) | $c/a$ | Volume (Å$^3$) |
|---|---|---|---|---|
| $\alpha$ | 4·75 | 12·97 | 2·74 | 253 |
| $\xi$ | 4·98 | 13·52 | 2·72 | 290 |
| $\xi'$ | 5·23 | ~ 14·12 | ~ 2·70 | ~ 333 |
| $\nu$ | 5·53 | 14·32 | 2·60 | 378 |
| $\mu$ | 5·60 | 13·67 | 2·44 | 371 |
| $\gamma$ | 5·59 | 13·69 | 2·45 | 372 |
| | 5·72 | 14·00 | 2·45 | 398 |

and volumes of the equivalent unit cells for the various phases are compared. The two values given for $\gamma$-alumina correspond to the limits given by Konig (1948) for the dimension of the cubic unit cell, which varies from 7·89 Å when excess aluminium is present, to 8·06 Å in the presence of excess oxygen.

The more-or-less regular increase in the values of $a$, $c$ and the volume, and decrease in the ratio $c/a$, in Table 2 suggests that the $\xi$, $\xi'$, $\nu$ and $\mu$ phases may be in some way intermediate between the $\alpha$ and $\gamma$ phases. For the $\alpha$-phase, the hexagonal cell contains 18 oxygen atoms, i.e. three atoms in each of the six close-packed oxygen layers. For the $\gamma$-phase the hexagonal cell contains 24 oxygen atoms, i.e. four atoms in each of six layers. Hence the increase in volume is mainly due to an increase in the number of oxygen atoms per layer, although the different co-ordination of the metal atoms makes the average volume per oxygen atom vary from 14·1 Å$^3$ for $\alpha$-alumina to 15·5 or 16·6 Å$^3$ for $\gamma$-alumina. These considerations suggest that, in the $\xi$ and $\xi'$ phases at least, there may be a mixture of four-atom-per-unit-cell and three-atom-per-unit-cell oxygen layers, so that there are between 18 and 24 oxygen atoms in a unit cell. The $\nu$ and $\mu$ phases may have the same arrangement of 24 oxygen atoms per unit cell as the $\gamma$-phase, but the large $c$ axis of the $\nu$-phase suggests that, in this case at least, some different arrangement of oxygen atoms is present.

### 3. The $\lambda$-phase

This phase, as stated above, is orthorhombic, but two of the axes are equal to within the limits of experimental error, so that it is pseudo-tetragonal with $a = b = 7{\cdot}63$, $c = 2{\cdot}89$ Å. The absence of a fourfold axis is evident from the lack of a fourfold symmetry in the intensities of the $hk0$ reflexions deduced from an examination of the pattern (Fig. 1) and a number of other similar patterns obtained with slightly different orientations of the crystal lattice. The space group has been identified as $D^5_h$–$Pmma$.

Single-crystal spot patterns corresponding to a wide variety of crystal orientations were observed. No preferred orientation with respect to the plane of the aluminium foil was indicated. For purposes of structure analysis, the best patterns obtained were those of $hk0$ and $2h,k,h$ spots obtained with the beam parallel to the [001] and [$\bar{1}$02] zone axes respectively. In each case the best possible set of relative intensities was deduced by correlating the visually estimated intensities of a number of patterns since none of the patterns was very good, some showing the effects of slight tilts of the specimen and others being partly obscured by reflexions from surrounding material. The sets of relative intensities so obtained were used to calculate [001] and [$\bar{1}$02] Patterson projections.

In addition to the sharp reflexions, most single-crystal patterns contained diffuse spots which were often elongated (see Fig. 2). Examination of many patterns showed that the diffuse spots could be attributed to the intersection of the Ewald sphere with a number of diffuse line-segments parallel to the $c^*$ axis of the reciprocal lattice. The central and strongest parts of the line segments occurred at points with indices which could be represented by $h,k\pm\delta,(2l+1)/2$ for integral $h$, $k$ and $l$. The value of $\delta$ obtained by measuring the microphotometer traces of the lines of diffuse spots in Fig. 2, was 0·289, or very nearly $\frac{2}{7}$. The scattering power along the line segments decreased from these positions to practically zero for integral $l$.

This distribution of diffuse line segments can be interpreted in terms of an imperfect superlattice structure in which the superlattice unit cell has dimensions $a$ in the $x$ direction, $7b$ in the $y$ direction and $2c$ in $z$ direction, with part of the structure factor of a normal unit cell varying approximately sinusoidally along the $y$ axis with a period of $3\frac{1}{2}$ unit cells. The sinusoidal variation must be 180° out of phase in successive unit cells along the $z$ direction. In terms of the superlattice cell, the sharp reflexions have indices $h,7k,2l$ and the diffuse reflexions have indices $h,7k\pm2,2l+1$.

In the initial stages of the structure analysis a fact which proved very useful was that the length of the $c$ axis, 2·89 Å, is close to the normal oxygen–oxygen distance in oxide structures. This limited the possible orientations of any tetrahedra or octahedra of oxygen atoms occurring in the structure.

A set of trial Fourier projections from $hk0$ reflexions consistently confirmed a zigzag chain of oxygen octahedra along the $x = \frac{1}{2}$ line in the $x\,y$ projection. Assuming this, additional oxygen atoms could be fitted into the unit cell only in a narrow strip along $x = 0$. If a row of oxygen atoms, about 2·8 Å apart, were placed approximately along the $y$ axis, there would be 2·7 oxygen atoms per unit cell. Such a row of oxygen atoms would be 'in phase' with the chain of octahedra along $x = \frac{1}{2}$ only once in every 7 unit cells or 19 oxygen atoms. This then could be the basis of the 7-unit-cell superlattice. The holes between the oxygen atoms along $x = 0$ and the oxygen atoms in

the octahedra, where metal atoms could be accommodated, would vary from unit cell to unit cell, so that the distribution of metal atoms would have a 7-unit-cell periodicity.

Trial Fourier projections of the average unit cell, based on this conception of the nature of the superlattice, showed, among other things, that there was a concentration of potential, too great to be accounted for by aluminium atoms only, around the $(0, \frac{1}{4})$ and $(0, \frac{3}{4})$ points in the [001] projection. In view of the evidence, described above, that the phase results from a reaction between aluminium and nickel oxides, it was assumed that these concentrations indicate the positions of nickel atoms in the structure.

### 4. The use of image-seeking methods

The application of image-seeking methods to the derivation of atomic arrangements from Patterson projections has been described by Buerger (1951), who discusses the use of a 'product function' or a 'minimum function', the latter being the more powerful. Such methods were applied to the interpretation of the [001] and [$\bar{1}02$] Patterson projections of the $\lambda$-phase in order to confirm the approximate structure derived by standard Fourier methods and to indicate the course of further refinement of the structure.

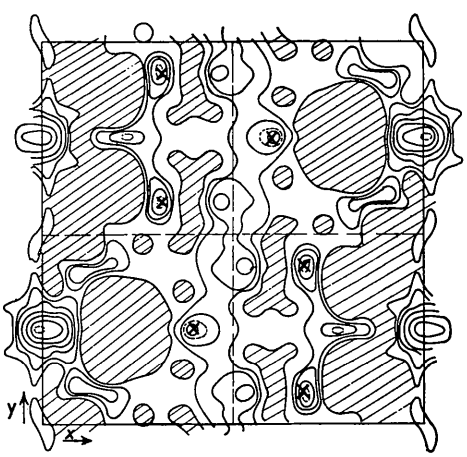


Fig. 6. The [001] projection of the $\lambda$-phase obtained by image-seeking, using the set of points indicated by crosses to scan the [001] Patterson projection. Negative areas are shaded.

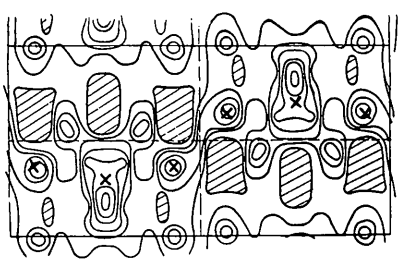

Fig. 7. The [$\bar{1}02$] projection of the $\lambda$-phase obtained by image-seeking on the [$\bar{1}02$] Patterson projection, using the set of points indicated by crosses.

Each Patterson projection was scanned with a set of points representing the positions of the oxygen atoms in the chain of octahedra along $x = \frac{1}{2}$, which was the feature of the structure most consistently confirmed by preliminary Fourier projections. For each position of the set of points relative to the Patterson projection, the minimum value of the Patterson function corresponding to a point of the set was recorded. The resulting projections of the structure are shown in Figs. 6 and 7. In each case the oxygen positions are confirmed and clear indications are given of the positions of the metal atoms.

Following the indications given by the projection (Fig. 6), the [001] projection of the structure was refined by a series of structure-factor calculations and Fourier summations in the usual way, and also by a method related to that previously used in the study of boric acid (Cowley, 1953c). In this method, the projection of the potential distribution of a crystal is represented by

$$V(x, y) = V'(x, y) + V''(x, y) ,$$

where $V'(x, y)$ is the approximate projection found by image-seeking or other methods, and $V''(x, y)$ is the 'error'. The Fourier transform of $V(x, y)$ is the structure-factor for electrons,

$$\mathcal{F} V(x, y) = E_{hk} = E'_{hk} + E''_{hk} .$$

For a centrosymmetric structure, the observed diffraction intensities give

$$E^2_{hk} = E'^2_{hk} + 2E'_{hk}E''_{hk} + E''^2_{hk} .$$

Then

$$E^2_{hk}/E'_{hk} = E'_{hk} + 2E''_{hk} + E''^2_{hk}/E'_{hk} ,$$

so that

$$\tfrac{1}{2}(E'_{hk} + E^2_{hk}/E'_{hk}) = E_{hk} + E''^2_{hk}/2E'_{hk} . \qquad (1)$$

Making the inverse transformation:

$$\mathcal{F}^{-1}\tfrac{1}{2}(E'_{hk} + E^2_{hk}/E'_{hk}) = V(x, y) + \mathcal{F}^{-1}(E''^2_{hk}/2E'_{hk}) . \qquad (2)$$

If $V''(x, y)$ is, in general, small compared with $V'(x, y)$, the second term on the right-hand side of (2)

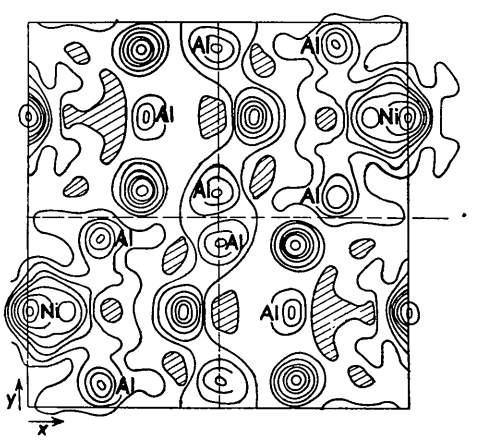


Fig. 8. The [001] projection of the $\lambda$-phase obtained by refining the projection (Fig. 6) by Fourier methods.

Table 3. *Comparison of observed and calculated structure factors for hk0 reflexions of the λ-phase*

| *hk* | $F_o$ | $F_c$ | *hk* | $F_o$ | $F_c$ | *hk* | $F_o$ | $F_c$ |
|---|---|---|---|---|---|---|---|---|
| 10 | 11 | 19 | 03 | 3 | 0 | 16 | 6 | 7 |
| 20 | 9 | 18 | 13 | 9 | 9 | 26 | 4 | 3 |
| 30 | 5 | 9 | 23 | 9 | −14 | 36 | 5 | − 1 |
| 40 | 9 | 15 | 33 | 8 | 7 | 46 | 4 | − 2 |
| 50 | 4 | − 4 | 43 | 9 | 10 | 56 | 4 | 5 |
| 60 | 6 | 8 | 53 | 6 | 3 | 66 | 4 | − 3 |
| 70 | 7 | 2 | 63 | 7 | − 8 | 76 | 4 | − 2 |
| 80 | 5 | − 5 | 73 | 7 | − 3 | 86 | 1 | 1 |
| 90 | 1 | − 5 | 83 | 1 | 3 | | | |
| | | | 93 | 2 | − 1 | 07 | 1 | 0 |
| 01 | 6 | 0 | | | | 17 | 4 | − 1 |
| 11 | 19 | −17 | 04 | 11 | 12 | 27 | 2 | − 2 |
| 21 | 16 | −18 | 14 | 6 | 4 | 37 | 2 | 4 |
| 31 | 15 | −17 | 24 | 9 | 6 | 47 | 3 | − 2 |
| 41 | 10 | 10 | 34 | 9 | 4 | 57 | 3 | − 1 |
| 51 | 5 | − 2 | 44 | 7 | − 4 | 67 | 2 | − 1 |
| 61 | 7 | − 7 | 54 | 6 | 6 | 77 | 2 | − 5 |
| 71 | 2 | 4 | 64 | 3 | − 2 | | | |
| 81 | 3 | − 1 | 74 | 4 | 3 | 08 | 8 | − 5 |
| 91 | 1 | − 1 | 84 | 1 | 2 | 18 | 4 | 2 |
| 10,1 | 1 | − 1 | | | | 28 | 4 | 3 |
| | | | 05 | 2 | 0 | 38 | 4 | 3 |
| 02 | 8 | − 6 | 15 | 3 | − 1 | 48 | 2 | − 5 |
| 12 | 20 | −23 | 25 | 8 | − 7 | 58 | 2 | 3 |
| 22 | 18 | −16 | 35 | 7 | − 7 | | | |
| 32 | 17 | −14 | 45 | 8 | 12 | 09 | 1 | 0 |
| 42 | 9 | 9 | 55 | 5 | 2 | 19 | 2 | − 3 |
| 52 | 8 | − 8 | 65 | 3 | − 6 | 29 | 1 | 3 |
| 62 | 5 | 8 | 75 | 6 | 5 | 39 | 1 | − 1 |
| 72 | 6 | − 4 | 85 | 4 | 2 | | | |
| 82 | 6 | − 4 | | | | 0,10 | 1 | − 5 |
| | | | 06 | 9 | −20 | 1,10 | 1 | 1 |

will be relatively small. It seems probable that it will not usually contain peaks resembling those of $V(x, y)$, but will give rise to an uneven background against which the $V(x, y)$ peaks stand out clearly. Hence it is possible to refine a projection by using as Fourier coefficients the values of $\frac{1}{2}(E'_{hk}+E^2_{hk}/E'_{hk})$ instead of the more usual $|E_{hk}|E'_{hk}/|E'_{hk}|$. The use of this method in the present case gave the more rapid convergence from the approximate to the final structure projection.

Equations similar to (1) and (2) hold for the electron density, $\varrho(x, y)$, and the structure-factors, $F_{hk}$, when X-ray diffraction data are used.

The final Fourier projection is shown in Fig. 8. For the purposes of structure-factor calculations, the distribution of possible nickel atom sites around the $(0, \frac{1}{4})$ and $(0, \frac{3}{4})$ positions was approximated by assuming fractions of nickel atoms to occur at several discrete points. If approximate average $z$ co-ordinates derived from the $[\bar{1}02]$ projection are added, the atomic co-ordinates used to calculate the final structure factors were as follows for the half unit cell from $y = 0$ to $y = \frac{1}{2}$:

O at (0·405, $\frac{1}{4}$, 0), (0·70, 0·075, $\frac{1}{2}$), (0·70, 0·425, $\frac{1}{2}$).
1·35 O distributed along $x = 0{\cdot}95$, $z = 0$.
$\frac{1}{2}$ Al at (0·505, 0·07, $\frac{1}{2}$), (0·505, 0·43, $\frac{1}{2}$), (0·19, 0·06, 0), (0·19, 0·44, 0).
$\frac{1}{8}$ Al at (0·69, $\frac{1}{4}$, 0).
$\frac{1}{4}$ Ni at (0, $\frac{1}{4}$, $\frac{1}{2}$).
$\frac{1}{4}$ Ni at (0·10, $\frac{1}{4}$, $\frac{1}{2}$).
$\frac{1}{10}$ Ni at (0·03, 0·19, $\frac{1}{2}$), (0·03, 0·31, $\frac{1}{2}$).

A comparison of the structure factors calculated for *hk*0 reflexions with those derived from the observed intensities is given in Table 3. The agreement may be considered satisfactory in view of the inaccuracies introduced by (1) the very rough nature of the estimates of the intensities of the spots; (2) the uncertainty as to the appropriate atomic scattering factor for the various ions at low angles of diffraction (Cowley, 1953*b*); (3) the use of fractional atoms at a few discrete points as an approximation for the average distribution of metal atoms in a unit cell; and (4) the presence of some secondary scattering, as shown by the appreciable intensities of the 'forbidden' 0*k*0 reflexions for $k$ odd. The approximate nature of the intensity estimates prevented any useful correction for secondary scattering (Cowley, Rees & Spink, 1951) from being made.

On the basis of the above distribution of atoms, the unit cell contains approximately 8·7 oxygen atoms, 4·67 Al and 1·40 Ni. The composition of the phase can therefore be represented by the formula $3\,NiO.5\,Al_2O_3$. This must be regarded as a rough estimate only.

Information on the relative positions of the metal atoms could be obtained only by consideration of the superlattice cell. The relative intensities of the diffuse spots occurring in the pattern (Fig. 2) were estimated visually and a Patterson projection covering 14 normal unit cells was calculated from them. This diffuse-spot Patterson projection could be regarded as a modulation to be applied to the $[\bar{1}02]$ Patterson projection previously obtained. The factor giving the

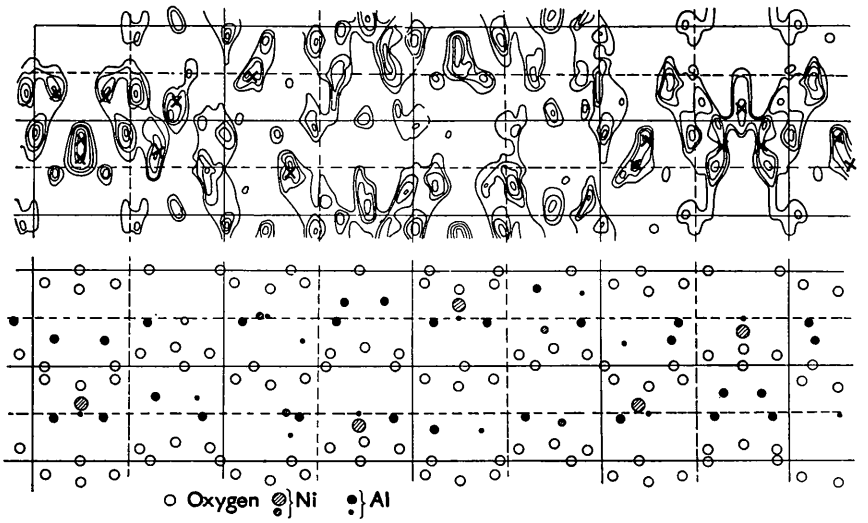


Fig. 9. The [$\bar{1}02$] projection of half the superlattice unit cell of the $\lambda$-phase obtained by image-seeking with the set of points indicated by crosses, with a diagram showing the atomic positions deduced from it. The relative sizes of the circles representing metal atoms indicate roughly the relative probabilities of metal atoms occurring at the points indicated.

relative strengths of the diffuse and sharp spots, and so determining the amplitude of the modulation of the Patterson function, could not be deduced from the pattern with any degree of accuracy, but was estimated from a knowledge of the fraction of the contents of the average unit cell which varied from cell to cell. Using this factor, the Patterson projections from the sharp and diffuse spots were added together to give a Patterson projection for the complete superlattice cell.

The application of image-seeking methods to this Patterson projection gave the [$\bar{1}02$] projection of the superlattice cell shown in Fig. 9 (in this figure the short axis of the projection has been expanded for convenience in plotting; consequently all peaks are extended in this direction). The set of points used for scanning the Patterson projection, 19 in all, was the set found from preliminary image-seeking experiments to correspond to the most prominent maxima in the projection. Only a little over half of the superlattice unit cell is shown in the figure. From Fig. 9 the main features of the superlattice structure could be deduced. These can best be appreciated by considering the [001]

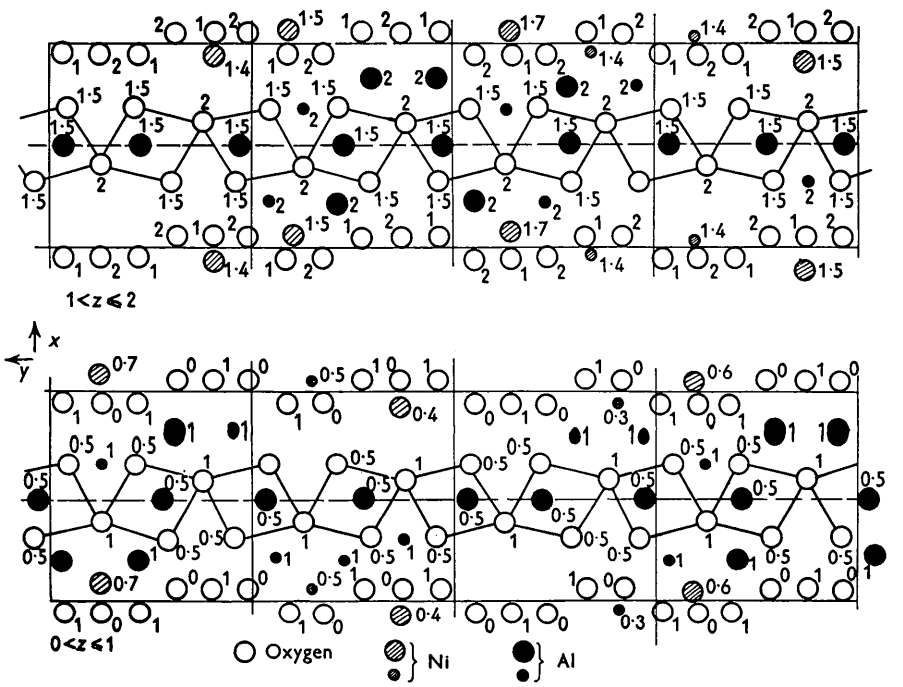


Fig. 10. The [001] projection of half the $\lambda$-phase superlattice unit cell deduced from Figs. 8 and 9, divided into two diagrams showing the arrangement of metal atoms for $0 < z \leq 1$ and $1 < z \leq 2$ respectively.

projection (Fig. 10). In discussion of the structure, co-ordinates are given in terms of the average unit-cell dimensions. Thus $z$ co-ordinates from 0 to 2 are given by figures near each atom.

The main features of the superlattice structure may be described as follows. The rows of oxygen atoms with $x = \pm 0{\cdot}05$ are 180° out of phase for $z = 0$ and 1. The possible sites for nickel atoms form four sets for which the approximate co-ordinates may be written $(0, n+\frac{1}{4}, \frac{1}{2})$, $(0, n+\frac{3}{4}, \frac{1}{2})$, $(0, n+\frac{1}{4}, \frac{3}{2})$ and $(0, n+\frac{3}{4}, \frac{3}{2})$ respectively. The probability of a site being occupied varies sinusoidally with a periodicity of $3\frac{1}{2}$ unit cells in the $y$ direction. Referred to variation of the probability of occupation of the $(0, n+\frac{1}{4}, \frac{1}{2})$ sites, the variation for the $(0, n+\frac{3}{4}, \frac{1}{2})$ and $(0, n+\frac{1}{4}, \frac{3}{2})$ sites is 180° out of phase, while the variation for the $(0, n+\frac{3}{4}, \frac{3}{2})$ sites is in phase. The probability of the aluminium sites at $x = \pm 0{\cdot}19$ and $x = \pm 0{\cdot}69$ being occupied has a similar variation with a $3\frac{1}{2}$-unit-cell periodicity. The variation for the aluminium sites with $z = 1$ is in phase with that of the nickel sites at $(0, n+\frac{1}{4}, \frac{1}{2})$, and that for the sites with $z = 0$ or 2 is 180° out of phase.

The most favoured nickel sites are enclosed in large tetrahedra of oxygen atoms formed when a triangle of oxygen atoms at $x = \pm 0{\cdot}05$ comes directly opposite one of the oxygen atoms at $\pm(0{\cdot}405, \frac{1}{4}, 0)$. The most favoured aluminium sites with $x = \pm 0{\cdot}19$ occur in tetrahedra formed by faces of the octahedra in the zigzag chain along $x = \frac{1}{2}$, and individual oxygen atoms along $x = \pm 0{\cdot}05$. The aluminium sites with $x = \pm 0{\cdot}69$ have octahedral co-ordination. The aluminium atoms with $x = \pm 0{\cdot}505$ alternate between the two tetrahedral sites associated with each octahedron, the choice being governed by the proximity of other metal atoms.

## 5. Conclusions

The atomic positions and the relative probability of occupation for the various metal sites in the superlattice unit cell have been determined very approximately. No attempt has been made to refine the projection of the superlattice cell obtained by image-seeking. The very rough nature of the estimation of intensities, and the uncertainties arising from the other causes listed previously, make it improbable that the large amount of labour involved in a refining process would lead to an appreciable increase in the amount of useful information on the structure. The methods used have been sufficient to show the general features of the structure, to indicate the approximate composition of the phase, and to provide a reasonable explanation for the formation of the superlattice in terms of the different periodicities of the chain of octahedra and the rows of oxygen atoms parallel to the $y$ axis.

Apart from being an indication that some reaction can take place between nickel oxide and alumina at temperatures as low as 450° C., the $\lambda$-phase probably has very little significance in itself. It has, however, provided a useful example of the amount of information which can be obtained from imperfect single-crystal electron-diffraction patterns, and of the application of image-seeking methods. In the case of the superlattice in particular, the image-seeking procedure alone has given all the information which could be expected from the limited data available. Hence it is to be expected that important progress could be made in the solution of many structural problems by the application of these methods. The series of oxides apparently intermediate between the $\alpha$- and $\gamma$-forms of alumina, mentioned above, and also the many forms of alumina reported in the literature as being produced by thermal treatment of hydrated alumina, form a field in which X-ray diffraction work is seriously limited by the small crystal size and imperfect ordering in many of the phases, but in which the application of electron-diffraction structure-analysis methods may prove very fruitful.

## References


Buerger, M. J. (1951). *Acta Cryst.* **4**, 531.

Cowley, J. M. (1953*a*). *Acta Cryst.* **6**, 53.

Cowley, J. M. (1953*b*). *Acta Cryst.* **6**, 516.

Cowley, J. M. (1953*c*). *Acta Cryst.* **6**, 522.

Cowley, J. M. & Rees, A. L. G. (1947). *Proc. Phys. Soc.* **59**, 287.

Cowley, J. M., Rees, A. L. G. & Spink, J. A. (1951). *Proc. Phys. Soc.* A, **64**, 609.

Konig, H. (1948). *Naturwissenschaften*, **35**, 92.

Krause, O. & Thiel, W. (1932). *Z. anorg. Chem.* **203**, 120.